General Disclaimer

One or more of the Following Statements may affect this Document

- This document has been reproduced from the best copy furnished by the organizational source. It is being released in the interest of making available as much information as possible.

- This document may contain data, which exceeds the sheet parameters. It was furnished in this condition by the organizational source and is the best copy available.

- This document may contain tone-on-tone or color graphs, charts and/or pictures, which have been reproduced in black and white.

- This document is paginated as submitted by the original source.

- Portions of this document are not fully legible due to the historical nature of some of the material. However, it is the best reproduction available from the original submission.

Produced by the NASA Center for Aerospace Information (CASI)

SATELLITE & MESOMETEOROLOGY RESEARCH PROJECT

Department of the Geophysical Sciences
The University of Chicago

A KINEMATIC INVESTIGATION OF THE INFLUENCE OF ANVIL AIR FLOW OVER
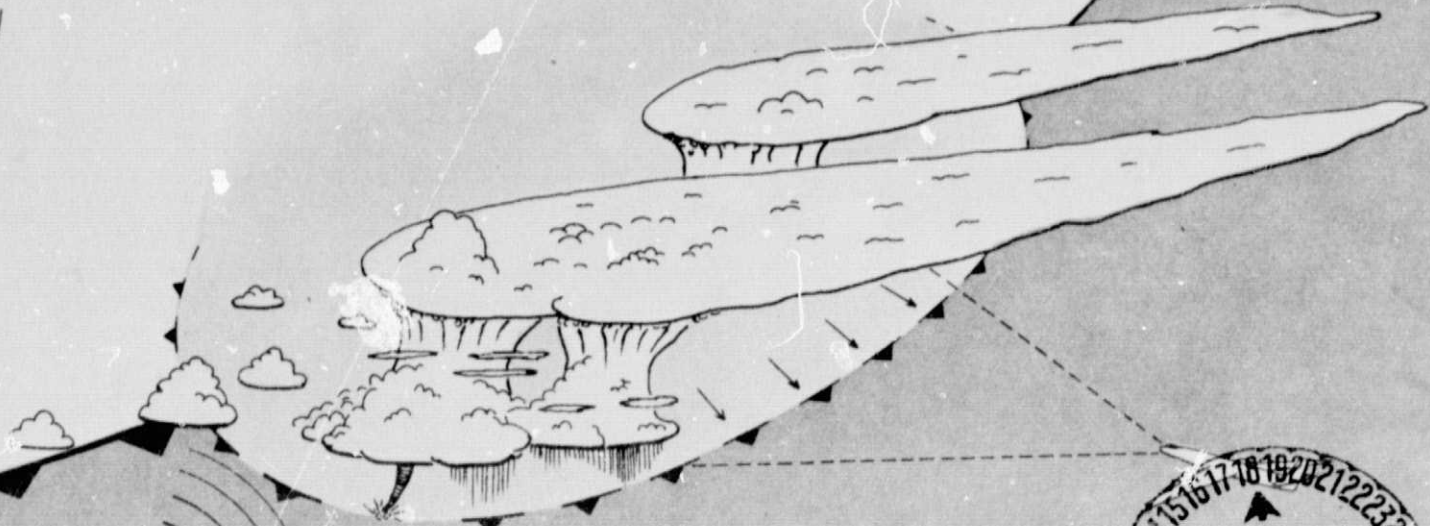# CONVECTIVE NEPHSYSTEMS ON HIGH-LEVEL HORIZONTAL FLOW

Ekundayo E. Balogun
Department of Physics, University of Ife
Ile-Ife, Nigeria

SMRP Research Paper
No. 160
July 1977

A KINEMATIC INVESTIGATION OF THE INFLUENCE OF ANVIL AIR FLOW OVER CONVECTIVE NEPHSYSTEMS ON HIGH-LEVEL HORIZONTAL FLOW

Ekundayo E. Balogun
Department of Physics, University of Ife
Ile-Ife, Nigeria

SMRP Research Paper No. 160

July 1977

A Kinematic Investigation of the Influence of Anvil Air Flow Over Convective Nephsystems on High-Level Horizontal Flow

Ekundayo E. Balogun
Department of Physics, University of Ife
Ile-Ife, Nigeria

ABSTRACT

The interactions between horizontal ambient flow and divergent wind fields, such as those that obtain atop cumulonimbus complexes, were investigated (theoretically) kinematically in this study. The following were observed from the results of the analyses. First, for a particular divergent field the relative mass flux over the area of the nephsystem decreased as the strength of the horizontal flow increased. Secondly, while in some of the cases analyzed the interaction between the two flows only resulted in the fanning out of streamlines and a slight redistribution in the wind speed, in many cases backflows and a total reorganization of the wind field occurred. Backflows have a blocking effect on the horizontal flow. Some of the computed patterns were compared with upper-level cloud vectors (from geostationary satellite photographs). The comparison indicated that the computed resultant wind field could be used to explain some features of such satellite-derived wind fields.

1. INTRODUCTION

Several investigations of thunderstorm complexes point to the fact that outflows from severe cumulonimbus clouds act to enhance or modify the upper-level flow. Results from investigations by Maclean (1961), Fujita and Bradbury (1969), Ninomiya (1971), Gaby and Poteat (1973), Chang and Tecson (1974), and Fujita (1974) etc., underscore the need for further investigation of the anvil airflow over thunderstorm complexes. Among other things, their investigations show that there is a relationship between vertical mass transport and the spreading rate of thundercloud anvils. The spreading rate is also, no doubt, influenced by the ambient wind. Studies of the anvil growth are, therefore, considered necessary for complete investigation of the interaction between small scale convective disturbance and large-scale atmospheric circulation--especially in the tropics. Information about the flow field at the anvil level is very necessary for the study of the interaction between high-level horizontal air flow and the diverging high clouds from thunderstorm complexes. One way of obtaining such information is by the use of time-lapse photographs of thunderstorm complexes from geostationary meteorological satellites.

Cloud photographs from geostationary satellites have been used successfully to estimate both low-level and high-level wind fields in the atmosphere. Examples of such computations are extant in the literature; for example, Fujita et al. (1968), Gaby and Poteat (1973), and Chang and Tecson (1974). The procedure involves tracing small elements of low-level and high-level clouds from time-lapse movie loops made from such cloud photographs. From these traces, estimates of low-level and upper-level wind fields are computed. From such satellite-derived wind fields, important characteristics of certain mesoscale and large-scale atmospheric systems have been obtained (see Fujita et al., 1968).

In the upper atmospheric regions (between 300 mb level and 200 mb level) over an area of convective nephsystems, the cloud velocities obtained by tracing elements of high-level clouds are the resultant flows between the ambient wind and the upper-level fields of cirrus outflows from convective nephsystems. However, the features of the resultant flows are usually not clearly established from winds

estimated from cloud motions, primarily because sufficient cloud elements could not be traced over the area of interest. A computed resultant wind is then desirable to give an insight into the influence of the upper-level winds over such nephsystems. The interaction between the ambient wind and the outflow often leads to the modification of both wind fields. The effect of such modification on the further development of the nephsystem has not been properly ascertained. Such information will certainly be useful for the further understanding of some features of nephsystems with overshooting tops. In this study some computations have been carried out to produce the general resultant flow configurations when an area of divergence is superimposed on a uniform flow. The resultant patterns are discussed vis-a-vis some results already obtained from actual computations of cloud velocities over nephsystems.

2. GENERAL PROCEDURE FOR COMPUTATIONS OF THE RESULTANT FLOW

The distribution of divergence over an area 600 km in diameter was as shown in Fig. 1. Six regions were demarcated by six concentric circles of radius r_n (n = 0, 1, 2, 3, 4, 5). The innermost region was assigned a divergence value D_o, which decreases linearly outwards to zero. It is assumed that in real situations, diverging cirrus outflow is strongest at the center of the system and weakens towards the outermost ring. Three values of D_o were used in the computation, viz 10^{-3} sec^{-1}; 10^{-4} sec^{-1}; 10^{-5} sec^{-1}. The innermost circle has a radius, r_o, equal to 50 km, and the subsequent circles--r_1, r_2, r_3, r_4, r_5 -- have radii equal to 100 km, 150 km, 200 km, 250 km, and 300 km, respectively.

These fields of divergence were superimposed on uniform horizontal flow - U_o = 5 m sec^{-1}, 10 m sec^{-1}, 25 m sec^{-1}, 50 m sec^{-1}, and 100 m sec^{-1}. The pairs D_o = 10^{-3} sec^{-1}, U_o = 100 m sec^{-1}, and D_o = 10^{-5} sec^{-1}, U_o = 5 m sec^{-1} represented a superimposition of a very strong horizontal flow over an area of strong divergence and a superimposition of a very weak divergence on a weak wind field. respectively. The flow fields representing these situations and the intermediate ones were computed. The characteristics of the mass flow in the general area of diverging winds were studied by considering the resultant flow along a common
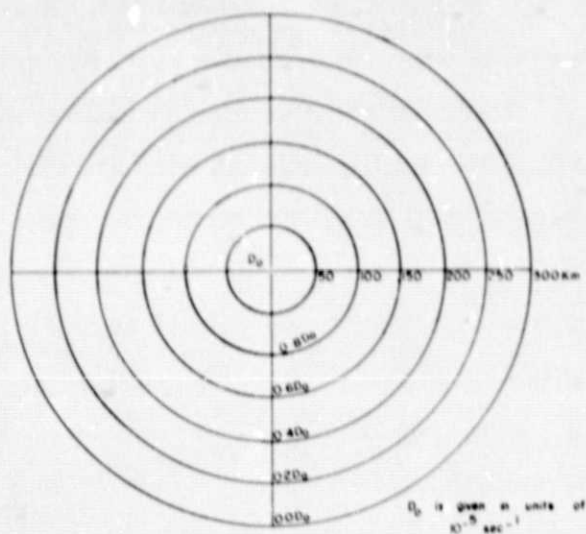
Fig. 1. Distribution of divergence
values used in computation.

diameter, XX[1], of the concentric circles in the general direction of the ambient
flow. The resultant flow along this diameter is normalized by the value of ambient
flow in each of the cases considered and plotted as a function of distance along each
diameter.

3. EXPRESSIONS USED IN COMPUTATIONS

To develop a working expression for computation of the diverging winds,
the following assumptions were made.

First, the region of the diverging winds was assumed to
be one kilometer thick.

Secondly, the radial velocities of the diverging flow was
assumed to be uniform both circumferentially and vertically
throughout the one kilometer layer.

Thirdly, the diverging winds were assumed to approximate
the behaviour of cirrus outflows from thunderstorm complexes.

Fourthly, it was assumed that the diverging pattern was stationary--no rotation or translation. The condition of no shear in the ambient flow was also assumed.

With these assumptions and with the use of the divergence theorem, the radial velocity, Vr_n, at each radial distance, r_n, was computed from the expression

$$Vr_n = Vr_{n-1} + \frac{2(r_n - r_{n-1})D_n}{r_n^2 - r_{n-1}^2},$$

where D_n is the value of D_0 at r_n.

4. RESULTANT FLOW AND HORIZONTAL MASS FLUX

The nature of a pure diverging streamline is shown in Fig. 2. When a uniform stream is superimposed on this, a resultant flow is computed at an azimuthal interval of ten degrees on each circle of radius r_n; that is, at thirty-six points on
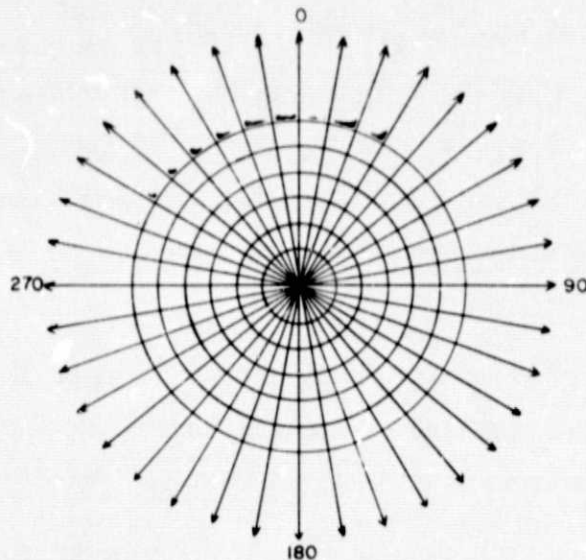

Fig. 2. Streamlines for pure
diverging winds.

each circle, using simple trigonometric relations. From the distribution of the magnitude and direction of these resultant winds, the resultant streamlines and isotachs are drawn for each situation considered. Because the patterns of resultant winds obtained are symmetric about the common diameter XX^1 of the concentric circles, only half of the patterns are shown in the upper-parts of Figs. 4-7.

As seen from the isotachs drawn on the patterns, the maximum and minimum resultant windspeeds occur along the common diameters XX^1. A graph of the normalized resultant wind U^* (normalized by the value of the ambient flow, that is $U^* = \frac{U_{XX^1}}{U_o}$) along the diameters XX^1 as a function of distance is shown in the lower parts of Figs. 4-7. If a unit distance perpendicular to XX^1 is considered in each case, then the curves will represent the mass flux along the diameters in the units of the mass flux transported by the uniform flow.

5. COMPUTED STREAMLINES

The resultant streamlines can be discussed under four broad categories: weak flow and weak divergence, weak flow and strong divergence, strong flow and weak divergence, and strong flow and strong convergence.

Before each category of streamline pattern is discussed, it is necessary to identify some points along xx^1 which will help in explaining some features of the resultant flow. These points are x_L, x_L^1, s, x_o, and O. Points s and x_o can only be identified in some of the patterns; in others, such points do not exist. These two points exist only in situations where the resultant flow exhibits a blocking effect.

Point S is a stagnation point and has the same meaning as in classical fluid mechanics. Point X_o is the apparent source of diffluent flow, and O is the origin of the pure divergent flow associated with each pattern.

The distance $X_L X_L^1$ denotes the extent along XX^1 of the influence of the interaction between the nephsystem and the flow. The length XX_L^1 varies from pattern to pattern, but in all cases it is greater than 600 km which is the diameter of the area of pure diverging winds.

In the schematic diagram shown in Fig. 3, a surface, Su, is defined by $S^1SS''S_o''S_oS^1$. This schematic representation illustrates the three dimensional features of a blocking-effect situation.
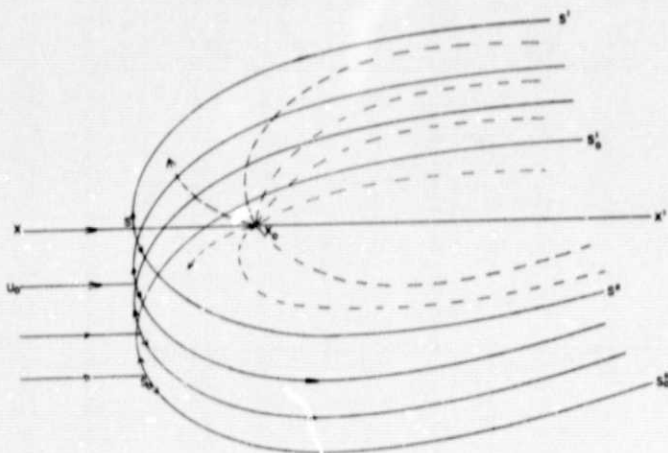
Fig. 3. Schematic representation of the
interaction between ambient flow and
the diverging flow.

Weak Flow and Weak Divergence

The streamlines obtained for the two cases--$D_o = 10^{-5}$ sec^{-1}, $U_o = 5$ m/s and $D_o = 10^{-5}$ sec^{-1}, $U_o = 10$ m sec^{-1} --represent the resultant flows for the condition of weak flow and weak divergence. In the first case, the upper part of Fig. 4A, there was a fanning out of streamlines in the general area of divergence. The isotachs show the distribution of the wind speed in the area of diverging winds. There is an upstream speed convergence and a concentration of generally more rapidly moving air downstream. This fact is also indicated by the graph of $U^* = \dfrac{U_{xx}^1}{U_o}$ against xx^1 in the lower part of Fig. 4. Convergence is indicated between -300 km and -150 km and also between 250 km and 300 km.

Weak Flow and Strong Divergence

The situations $D_o = 10^{-4}$ sec^{-1}, $U_o = 5$ ms^{-1}; $D_o = 10^{-4}$ sec^{-1}, $U_o = 10$ m s^{-1}; $D_o = 10^{-3}$ sec^{-1}, $U_o = 5$ m s^{-1}; and $D_o = 10^{-3}$ sec^{-1}, $U_o = 10$ m s^{-1}

8
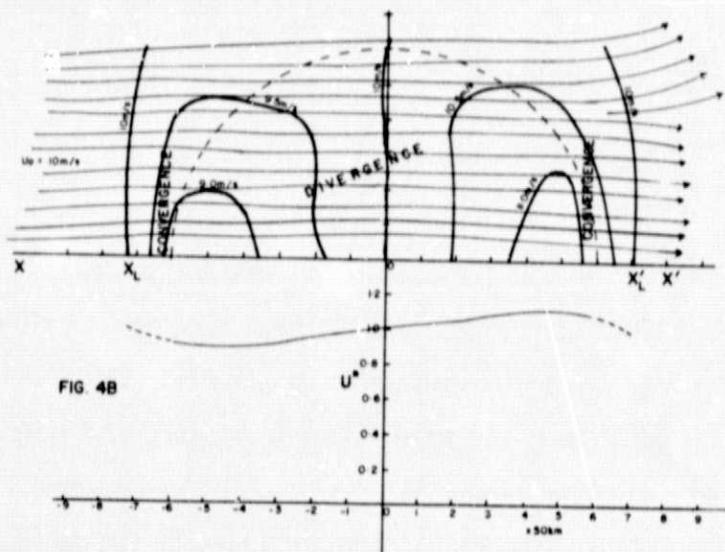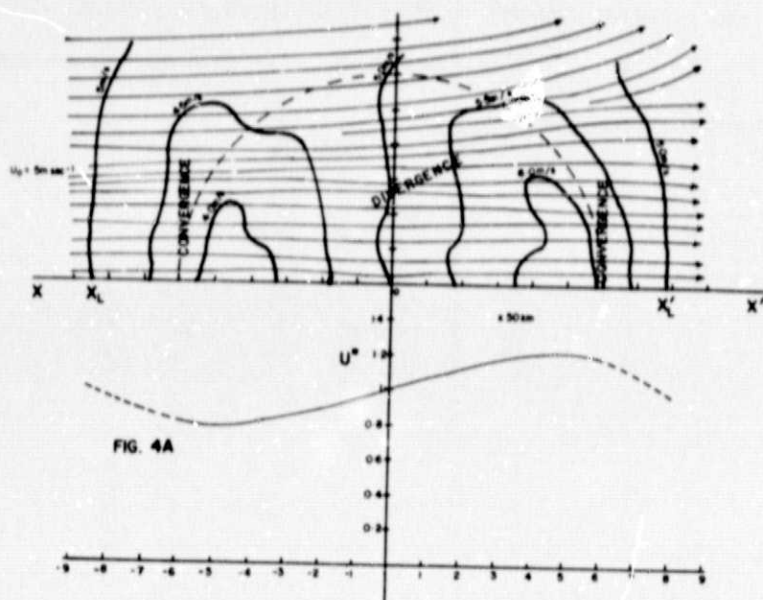
Fig. 4. Streamline patterns for the situations
$D_o = 10^{-5}$ sec^{-1}, $U_o = 5$ m sec^{-1} (4A) and
$D_o = 10^{-5}$ sec^{-1}, $U_o = 10$ m sec^{-1} (4B).
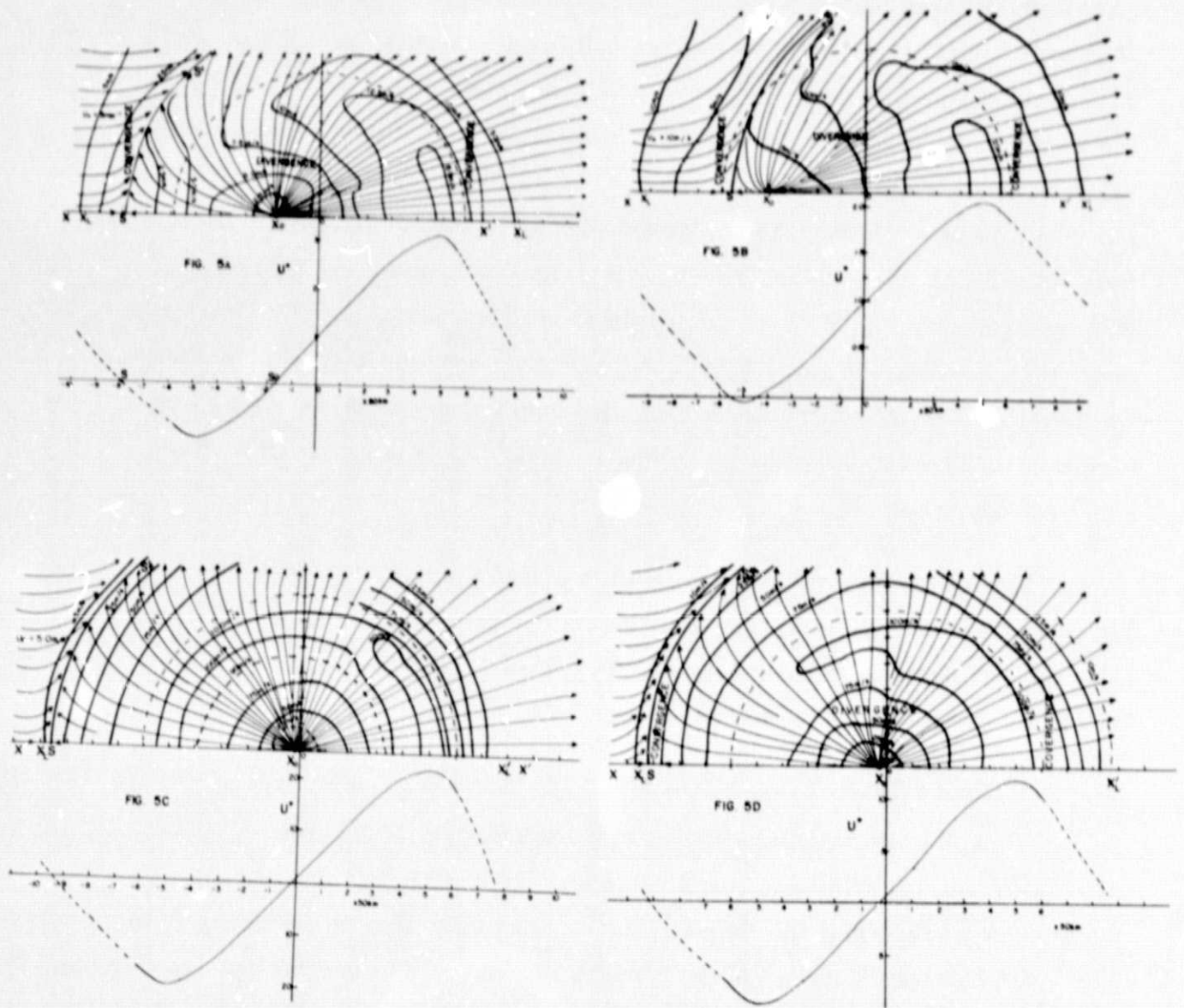
Fig. 5. Streamline patterns for the following situations:

$D_o = 10^{-4}$ sec^{-1} , $U_o = 5$ m sec^{-1} (5A); $D_o = 10^{-4}$ sec^{-1} , $U_o = 10$ m sec^{-1} (5B);

$D_o = 10^{-3}$ sec^{-1} , $U_o = 5$ m sec^{-1} (5C); $D_o = 10^{-3}$ sec^{-1} , $U_o = 10$ m sec^{-1} (5D).

represent this condition. In all these cases, the areas of diverging air show a blocking effect (see Fig. 5). The general configuration is similar to a profile of a plane half-body produced when a line source is superimposed on a uniform stream. For these configurations, there is a point identified as S along xx^1 where the velocity of the diverging air will be equal in magnitude but opposite in direction to that of the uniform stream. The combined velocity is zero at that point. In classical fluid mechanics such points are identified as stagnation points, and to carry the analogy further the line XSS^1 is akin to the stagnation streamline. That is, the streamline XS does not end at S but continues to S^1 and similarly to S^{11} which is an image of S^1 on the other side of XX^1. Physically then, all the diverging flow will be confined inside a surface S_u defined by $S^1SS^{11}S_o^{11}S_oS_o^1$, as illustrated schematically in Fig. 3.

In classical fluid mechanics, the flow inside S_u is ignored and it is assumed that the surface S_u can be replaced by a solid body while the flow outside S_u still retains its configuration. In this study, however, both the flow inside and outside S_u are of importance.

Strong Flow and Weak Divergence

This situation is represented by the conditions $D_o = 10^{-5}$ sec^{-1}, $U_o = 25$ m sec^{-1}, 50 m sec^{-1}, and 100 m sec^{-1} (see Fig. 6). In these cases, evidence of the diverging flow in the resultant streamline flow is all but wiped out. In all cases, however, the resultant isotachs show that the horizontal flow has been strengthened. There is speed convergence upstream and speed divergence downstream.

Strong Flow and Strong Divergence

The cases $D_o = 10^{-3}$ sec^{-1}, 10^{-4} sec^{-1} and $U_o = 25$ m sec^{-1}, 50 m sec^{-1}, 100 m sec^{-1} represent the condition of strong divergence and strong ambient flow. The streamlines depicting this situation are shown in Fig. 7. When $D_o = 10^{-4}$ sec^{-1} the resultant streamlines showed a diffluent flow. The spreading of the streamlines becomes less pronounced with increase in the speed of the ambient wind. When the
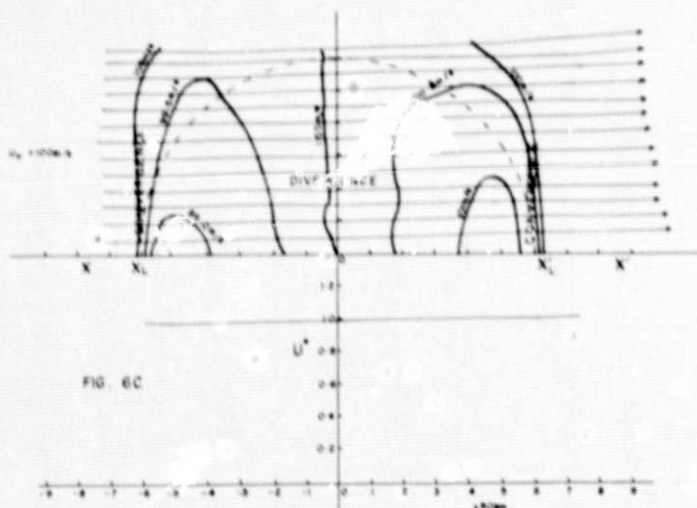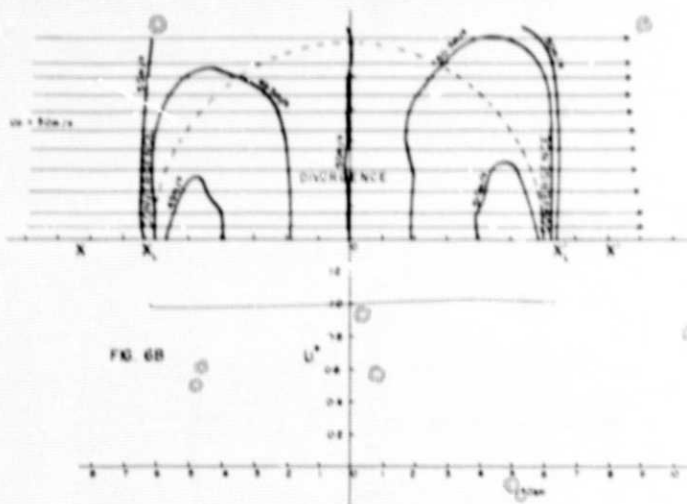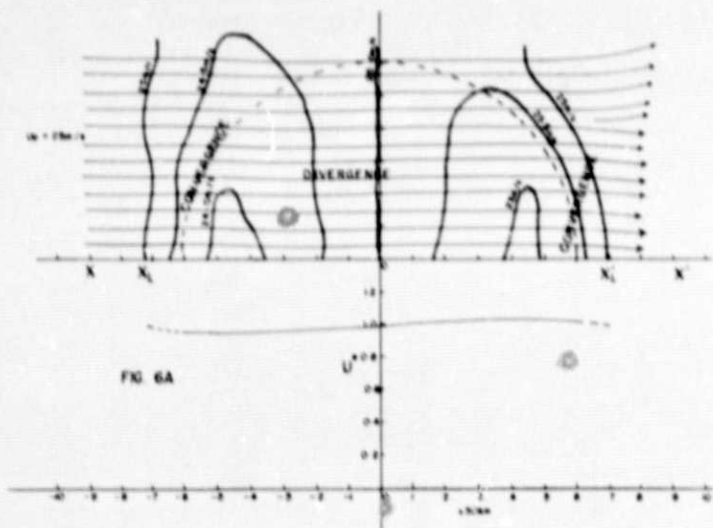
FIG. 6A

FIG. 6B

FIG. 6C

Fig. 6. Streamline patterns for the
following situations, respectively:

$D_o = 10^{-5}$ sec^{-1} , $U_o = 25$ m sec^{-1} (6A);

$D_o = 10^{-5}$ sec^{-1} , $U_o = 50$ m sec^{-1} (6B);

$D_o = 10^{-5}$ sec^{-1} , $U_o = 100$ m sec^{-1} (6C).

divergence is one order of magnitude stronger, i.e. 10^{-3} sec^{-1}, the resultant flow
field is different. There is a "blocking" of the ambient flow and the general
characteristics of the flow is similar to the cases of weak flow and strong divergence.

6. SATELLITE-DERIVED UPPER-LEVEL WINDS OVER NEPHSYSTEMS

Figure 8 shows the photograph of a diamond-shaped thunderstorm complex
in the midwestern United States (between 30-35 degrees N latitude and 95-100
degrees W longitude) from a digitized ATS picture. Computation of two-dimensional
mass flux over the thunderstorm complex by Fujita and Bradbury (1969) is repro-
duced in Figs. 9a and 9b. Figure 9b shows the motion of high clouds over the

complex, relative to radar echoes from the complex. Mass fluxes were computed along the lines A, B, C, ... M, which are orthogonal trajectories to the smooth relative streamlines shown in Fig. 9ª. Fujita and Bradbury suggested that the
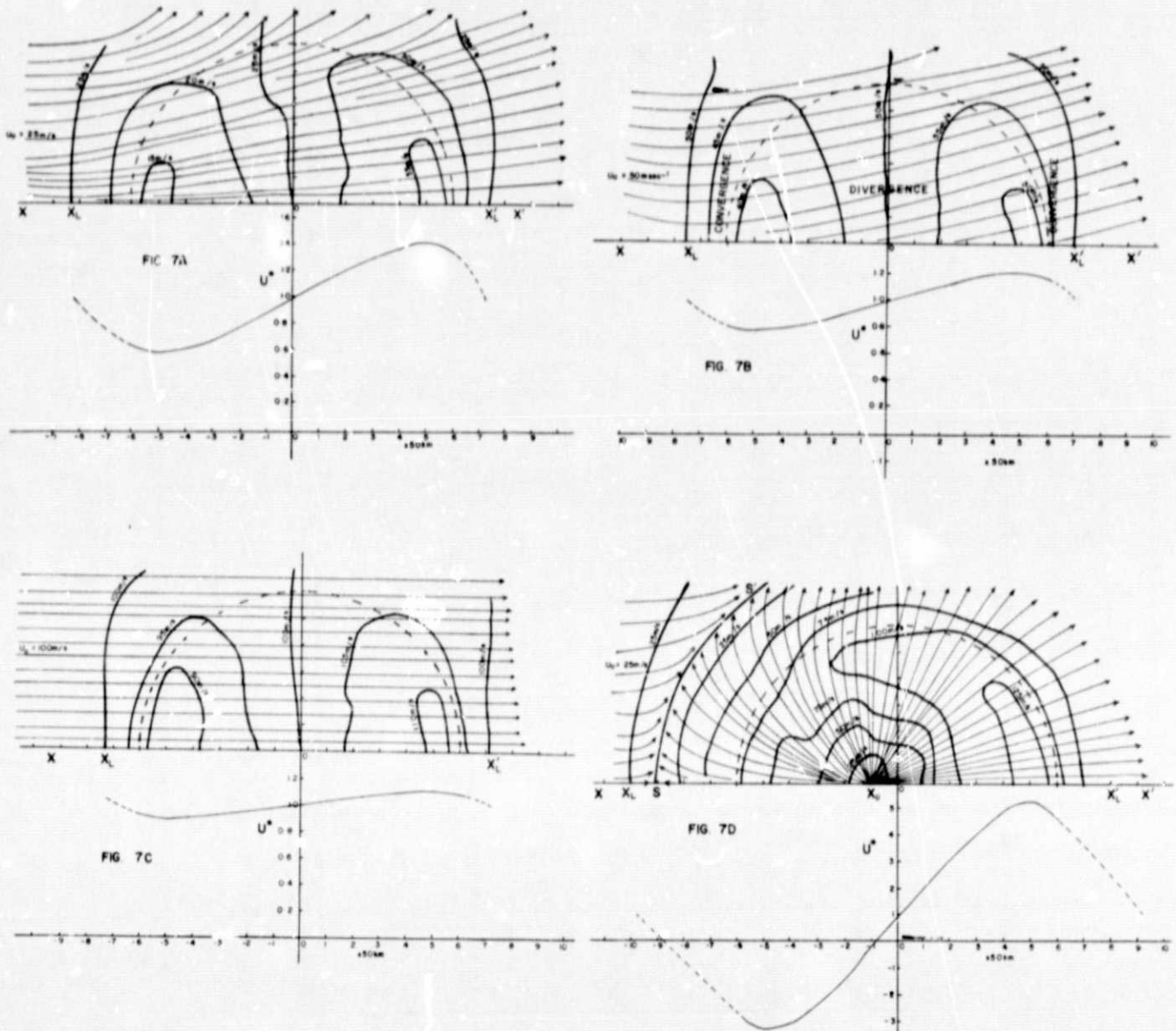

Fig. 7. Streamline patterns for the following situations:

$D_o = 10^{-4}$ sec^{-1} , $U_o = 25$ m sec^{-1} (7A); $D_o = 10^{-4}$ sec^{-1} , $U_o = 50$ m sec^{-1} (7B);

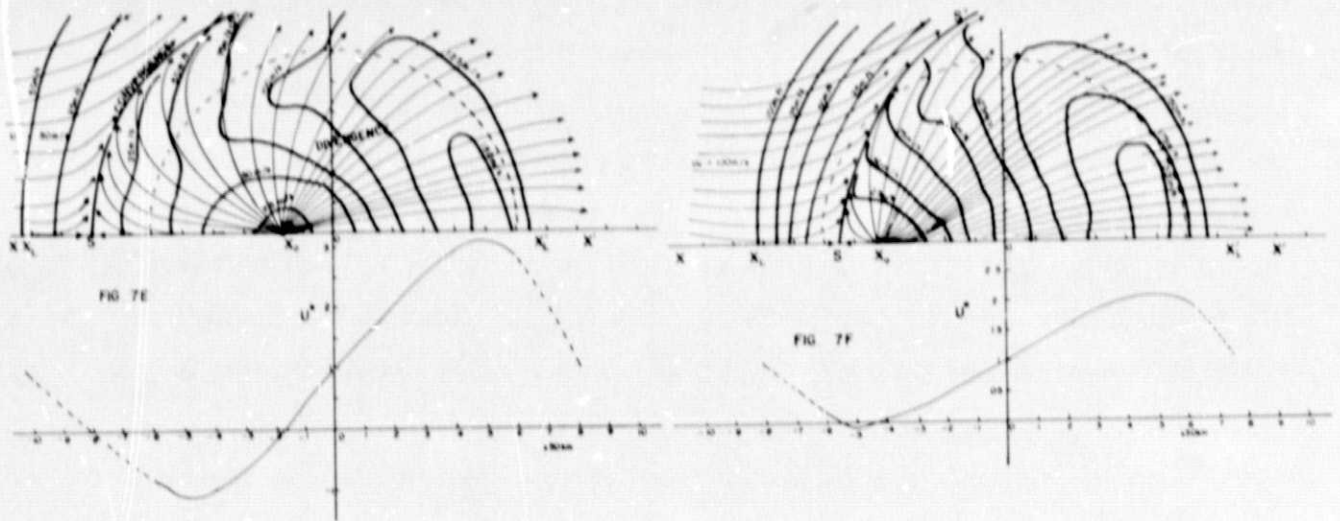$D_o = 10^{-4}$ sec^{-1} , $U_o = 100$ m sec^{-1} (7C); $D_o = 10^{-3}$ sec^{-1} , $U_o = 25$ m sec^{-1} (7D);

Fig. 7. (Cont'd) Streamline patterns for the following situations:

$D_o = 10^{-3} \ sec^{-1}$, $U_o = 50 \ m \ sec^{-1}$ (7E); $D_o = 10^{-3} \ sec^{-1}$, $U_o = 100 \ m \ sec^{-1}$ (7F).

Fig. 8. Photograph of a diamond-shaped thunderstorm
complex in the midwestern United States.

reduction in mass flux from line A to line D, before the major convective area was reached, was due to a blocking effect. The mass flux increased from D to M over the convective nephsystem. The situations depicted in Figs. 8, 9a, and 9b are, perhaps, similar to the situation of fairly strong horizontal winds (i.e., 10-25 m sec^{-1}), overrunning a strong diverging anvil-level flow; as shown in Figs. 5b and 7a for example. In the upper part of Fig. 5b two flows separated by SS^1 are observed. The maximum speed to the right of SS^1 is 20 m sec^{-1}. There is also a small backflow between S and X_o. This backflow is indicated as "negative" flux in the lower part of the figure. If the flow along XX^1 is considered, it is observed that as the divergence area is approached the mass flux is reduced gradually until the region of backflow is reached. After the area of backflow, there is a general increase in the mass flux. The mass flux increases to a maximum downstream. In the upper part of Fig. 7a, a backflow is not exhibited but a general reduction in the mass flux is observed as the area of 'nephsystem' is approached, and an increase in the mass flux is observed downstream.

For the computed streamlines in all cases, there is a general reduction in the mass flux as the area of nephsystem is approached and an increase in the mass flux downstream. Backflows are only observed in cases of very strong divergence and weak- to moderately-strong horizontal flows.

Figures 10 and 11 (from Chang and Tecson, 1974) also show cloud motions at high levels. They show the resultant flow between high-level flows and upper-level divergence fields associated with nephsystems. In these observed cases, it is not possible to obtain the kind of details one obtains with the computed patterns. The computed patterns can, however, serve as guides to the interpretations of these satellite-observed patterns.

7. CONCLUDING REMARKS

From the foregoing discussion, it is noted that outflows from thunderstorm complexes often make an impression on the existing flow field at high levels. In some cases, such impressions are not apparent in the streamlines but are very
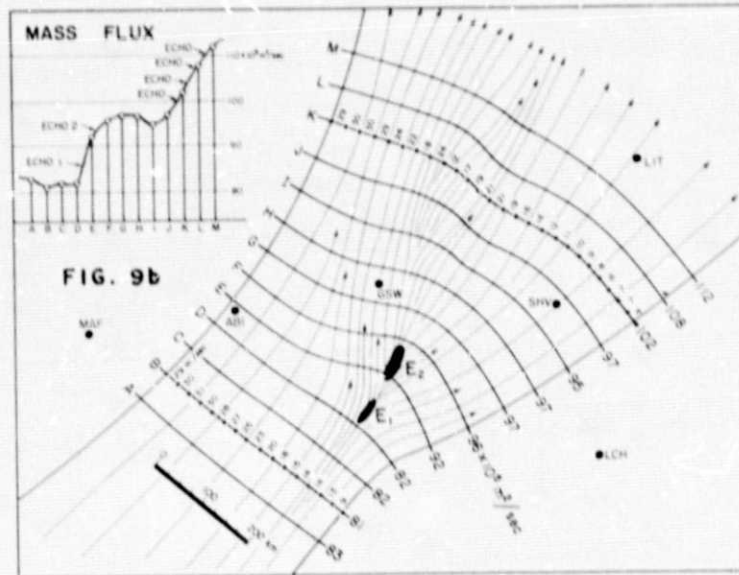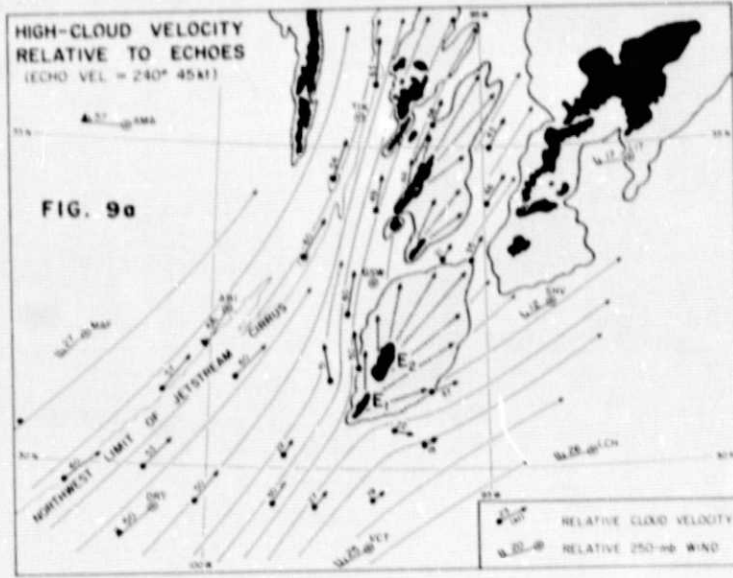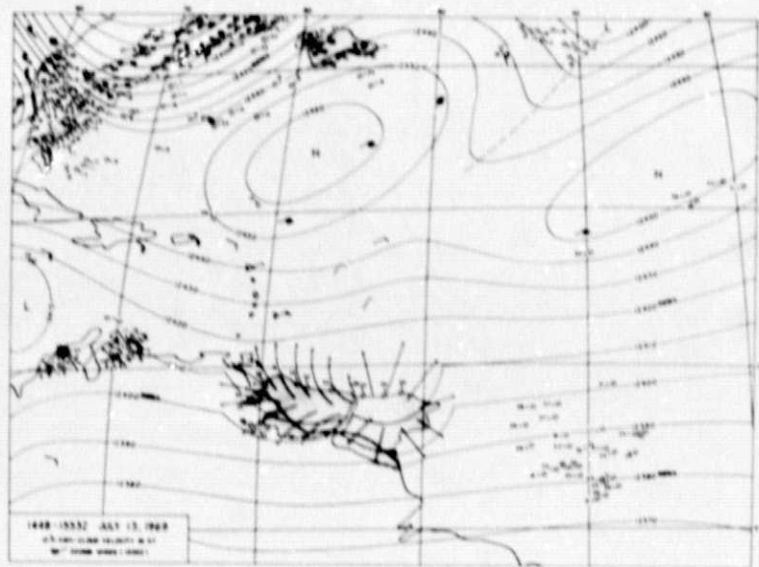
Figs. 9a and 9b. Computations from Fig. 8.

Fig. 10. Some computations of cloud motions over some nephsystems over the Atlantic Ocean from ATS photographs. (From Chang and Tecson, 1974)

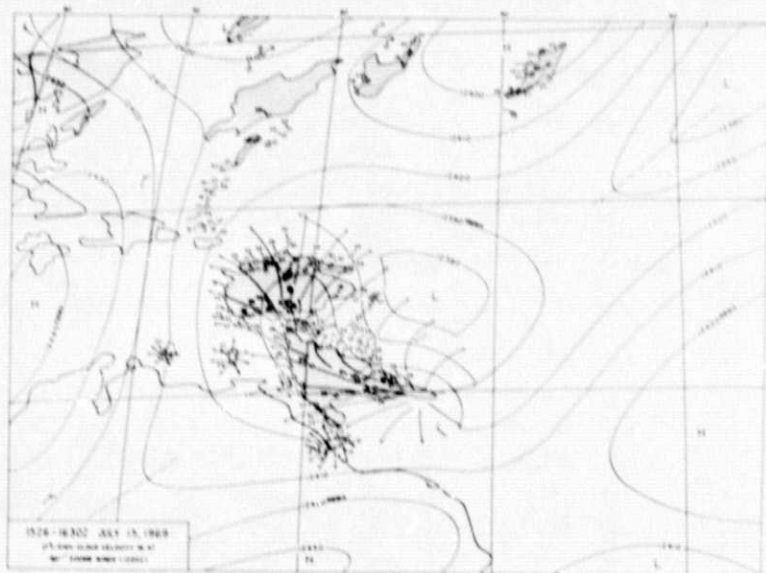

Fig. 11. Other computations of cloud motion over nephsystems over the Atlantic Ocean from ATS photographs. (From Chang and Tecson, 1974)

noticeable in the distribution of the windspeeds. In other cases, the resultant interaction manifests itself both as changes in the direction of flow and also in the distribution of the windspeed. Although the present analyses are purely kinematic, yet there have been observations on cloud scales, both dynamical and thermodynamical, which suggest (see Maclean, 1961 and Ninomiya, 1971) that some severe cumulonimbus clouds act to enhance the upper-level flow.

The salient points observed from the results of the kinematic analysis are:

First, for a particular divergence field, D_O, the relative mass flux over the area of nephsystem decreases as the strength of the horizontal flow increases.

Secondly, conditions of backflows occur over areas of strong divergence and relatively weak upper-level winds. See Figs. 5a, 5d, and Figs. 7d-7f. In cases of backflow, it is noted that the 'source' X_O was located to the left of the 'source' O of a pure diverging flow on which the uniform horizontal flow was superimposed.

Thirdly, the backflows have a blocking effect on the horizontal flow. In these cases, the distance between the apparent source X_O of the backflow and the center of the pure diverging flow, O increases with increasing ambient flow for a particular divergence field D_O.

The questions that come to mind after carrying out these analyses are: Do nephsystems have a better chance of development in areas where the existing upper winds are light than at locations where there are winds of jet speeds? Do very severe convective activities occur in situations of backflows? These questions cannot be answered from purely kinematic analyses. Only a combination of dynamical and thermodynamical analyses of well-documented cases of interaction between anvil air flow and ambient wind can throw some light on these questions.

REFERENCES

Chang, Y. M. and J. J. Tecson, 1974: Cloud Velocities Over the North Atlantic Computed from ATS Picture Sequences. SMRP Research Paper 121. The University of Chicago.

Fujita, T. T., K. Watanabe, and T. Izawa, 1969: Formation and Structure of Equatorial Anticyclones caused by Large-scale Cross Equatorial Flows Determined by ATS-1 Photographs. SMRP Research Paper 78. The University of Chicago.

Fujita, T. T. and D. L. Bradbury, 1969: Determination of Mass Outflow from a Thunderstorm Complex Using ATS III Pictures. SMRP Research Paper 79. The University of Chicago.

Fujita, T. T., 1974: Overshooting Thunderheads Observed from ATS and Learjet. SMRP Research Paper 117. The University of Chicago.

Gaby, D. C. and K. O. Poteat, 1973: ATS-3 Satellite-Derived Low-Level Winds. A Provisional Climatology. J. of Appl. Met., 12, 1054-1061.

Maclean, G. S., 1961: Observation of a Severe Convective Activity on a Squall Line. Bull. Amer. Met. Soc., 42, 252.

Ninomiya, K., 1971: Dynamical Analysis of Outflow from Tornado-Producing Thunderstorm as Revealed by ATS III Pictures. J. Appl. Met., 10, 275.